Available online at www.sciencedirect.com
SCIENCE DIRECT®
Physica D 195 (2004) 303–323
PHYSICA D
www.elsevier.com/locate/physd

Interaction of sine-Gordon kinks with defects: the two-bounce resonance

Roy H. Goodman [a,*], Richard Haberman [b]

[a] *Mathematical Sciences Department, New Jersey Institute of Technology, Newark, NJ 07102, USA*
[b] *Department of Mathematics, Southern Methodist University, Dallas, TX 75275, USA*

Abstract

A model of soliton–defect interactions in the sine-Gordon equations is studied using singular perturbation theory. Melnikov theory is used to derive a critical velocity for strong interactions, which is shown to be exponentially small for weak defects. Matched asymptotic expansions for nearly heteroclinic orbits are constructed for the initial value problem, which are then used to derive analytical formulas for the locations of the well known two- and three-bounce resonance windows, as well as several other phenomena seen in numerical simulations.

Keywords: Sine-Gordon kinks; Two-bounce resonance; Singular perturbation theory

1. The two-bounce resonance and related phenomena

The two-bounce resonance is a phenomenon displayed by many non-integrable systems in which a solitary wave interacts either with another solitary wave or else with a localized defect in the medium through which it propagates. Fei et al. study the two-bounce resonance in the sine-Gordon equation perturbed by a localized nonlinear defect [1]:

$$u_{tt} - u_{xx} + \sin u = \epsilon\delta(x)\sin u. \tag{1.1}$$

Kink solitons are initialized propagating (numerically) toward a defect with incoming velocity v_{in} and allowed to interact with the defect. Then one of two things might happen: either the soliton is trapped and comes to rest at the defect location, or else it escapes and propagates away at outgoing velocity v_{out}. (The soliton cannot be destroyed by the interaction because it is defined by its boundary conditions at infinity.) They find that there exists a critical velocity v_{c}. Kink solitons with initial velocity greater than v_{c} pass by the defect. Most solitons with initial speeds below the v_{c} are trapped, remaining at the defect for all times after the interaction time. However, there exist bands of initial velocities, known as resonance windows, for which the kink is reflected by the defect, rather than being trapped. This is summarized in Fig. 1, taken from their paper.

* Corresponding author. Tel.: +1-973-6424261; fax: +1-973-5965591.
E-mail address: goodman@njit.edu (R. Haberman).

0167-2789/$ – see front matter © 2004 Elsevier B.V. All rights reserved.
doi:10.1016/j.physd.2004.04.002

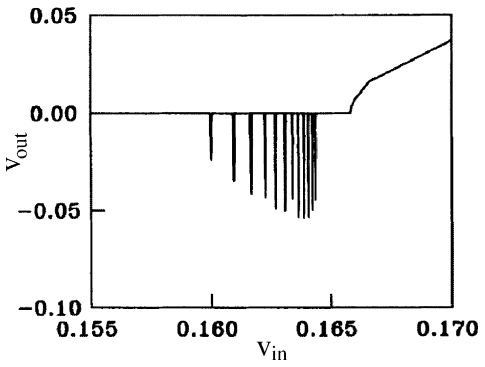

Fig. 1. The output vs. input velocities of sine-Gordon solitons interacting with a delta-well defect, from [1], reprinted with permission.

A phenomenological explanation for this phenomenon (in the context of kink–antikink interactions in various nonlinear Klein–Gordon equations) was given in a series of of papers by Campbell and coworkers [2–5].[1] They use very elegant physical reasoning to argue that the reflection windows are due to a resonant interaction between the movement of the kink–antikink pair in an effective potential, and shape modes oscillating about the kinks. Fei et al. adapt this reasoning to analyze the two-bounce resonance phenomenon in the sine-Gordon equation, using a variational approximation to reduce the PDE to a pair of second order ODE, and use a similar argument to find the resonance windows. Both these studies make the assumptions that the resonance takes a certain form, dependent on unknown constants, and use physical reasoning and statistical data fitting to find these constants.

An inspiration for the present work comes from one of the authors' previous studies of the trapping of gap solitons in Bragg grating optical fibers with defects [6]. In that study, sufficiently slow solitons in certain parameter regimes were captured by localized defects. This previous work does not offer a mechanism to explain the existence of a critical velocity for soliton capture, which we are now able to explain for the simpler model problem discussed here. The two-bounce resonance phenomenon is also seen by Tan and Yang in simulations of vector solitons collisions in birefringent optical fibers [7].

The aim of the current paper is to make mathematically precise the physical reasoning of the previous studies of the two-bounce resonance, in a way that does not rely on statistical inference. We analyze the variational ODE model derived in [1] using the methods of singular perturbation theory to match a nonlinear saddle to nearly heteroclinic orbits in a manner similar to that previously used by Haberman [8,9] and Diminnie and Haberman [10,11]. The critical velocity is determined via a Melnikov integral and the location of the resonance windows arises naturally due to a matching condition in the expansion. Intriguingly, finding the critical velocity requires that we make use of terms which are small beyond all orders in ϵ in the matched asymptotic expansion, as was done, notably, by Kruskal and Segur [12], and by many others.

Other work on soliton dynamics in perturbed sine-Gordon equations is summarized by Scott [13]. In this approach, an ordinary differential equation is derived for the evolution of the Hamiltonian, which can then be related to the soliton's velocity. McLaughlin and Scott [14] study a damped and driven sine-Gordon system modeling a Josephson junction and find a unique limiting velocity for solitons under that perturbation. The fundamental difference between their system and ours is the presence of the localized defect mode, which must be included in the reduced system.

[1] The phrase *two-bounce resonance* was coined in these papers to describe the following situation. Kinks with velocity above a critical value collided once, then separated and moved off to infinity. Kinks in the reflection windows collided and moved apart slightly, then turned around and collided a second time before separating fully and escaping to infinity at constant velocity. The physical situation in the present case is somewhat different, but, as the mechanism is essentially the same, we keep the terminology.

The paper is laid out as follows. In Section 2 we introduce a system of ordinary differential equations that models Eq. (1.1), and show the results of numerical simulations of the model. In Section 3, we determine the critical velocity separating captured kinks from those that pass by the defect. In Section 4, we derive formulas that are valid in a neighborhood of $|X| = \infty$. These are used in Section 5 where we construct matched asymptotic expansions to solutions satisfying the two-bounce resonance. We find the sequence of velocities defining the resonance windows, as well as formulas for the window widths. We also find locations of three-bounce resonance windows and approximations for the general initial value problem. In Section 6, we demonstrate the validity of this approach by comparing the formulas derived in the previous two sections with the results of numerical simulations. We summarize and include a more general discussion in Section 7.

2. The variational approximation

Following Fei et al. [1], we consider a sine-Gordon model with a localized impurity at the origin, given by Eq. (1.1). In the absence of any impurity, i.e. $\epsilon = 0$, the sine-Gordon equation has the well-known family of kink solutions parameterized by velocity v:

$$u_k(x,t) = 4\tan^{-1}\exp\left(\frac{x - vt - x_0}{\sqrt{1-v^2}}\right).$$

If we consider the system with an impurity, then solutions of small amplitude approximately satisfy the linear equation:

$$u_{tt} - u_{xx} + u = \epsilon\delta(x)u, \tag{2.1}$$

which, for $0 < \epsilon < 2$, has standing wave solutions

$$u_{\mathrm{im}}(x,t) = a(t)\,\mathrm{e}^{-\epsilon|x|/2},$$

where $a(t) = a_0\,\cos(\Omega t + \theta_0)$ and

$$\Omega = \sqrt{1 - \frac{\epsilon^2}{4}}. \tag{2.2}$$

Fei et al. [1] study the interaction of the kink and defect modes using a variational approximation to derive a set of equations for the evolution of the kink position X, and the defect mode amplitude a. An excellent review of the use of variational approximations in nonlinear optics is given by Malomed [15]. To derive the approximate equations, they substitute the ansatz

$$u = u_k + u_{\mathrm{im}} = 4\tan^{-1}\exp(x - X(t)) + a(t)\,\mathrm{e}^{-\epsilon|x|/2} \tag{2.3}$$

into the Lagrangian of (1.1)

$$L = \int_{-\infty}^{\infty}\left(\frac{1}{2}u_t^2 - \frac{1}{2}u_x^2 - [1 - \epsilon\delta(x)](1 - \cos u)\right)\mathrm{d}x. \tag{2.4}$$

Here X replaces $x_0 + vt$, and a and X, the parameters characterizing the approximate solution (2.3), are regarded as unknown functions of t. It is assumed that a and ϵ are small enough that many cross-terms can be neglected. Thus, in calculating the effective Lagrangian, all terms produced via overlap of the two modes are neglected, excepting those which include the defect potential $\delta(x)$. This is equivalent to assuming that the dominant means of

interaction between the two modes is via the defect. Evaluating the spatial integrals of (2.4), an effective Lagrangian $L_{\text{eff}}(X, a, \dot{X}, \dot{a})$ is obtained [1]:

$$L_{\text{eff}} = 4\dot{X}^2 + \frac{1}{\epsilon}(\dot{a}^2 - \Omega^2 a^2) - \epsilon U(X) - \epsilon a F(X), \tag{2.5}$$

where

$$U(X) = -2\text{sech}^2(X), \qquad F(X) = -2\tanh(X)\text{sech}(X).$$

The corresponding evolution equations are then given by the classical Euler–Lagrange equations for (2.5):

$$8\ddot{X} + \epsilon U'(X) + \epsilon a F'(X) = 0, \tag{2.6a}$$

$$\ddot{a} + \Omega^2 a + \tfrac{1}{2}\epsilon^2 F(X) = 0. \tag{2.6b}$$

This system has also been studied in [16]. Note that the system conserves the Hamiltonian

$$H = 4\dot{X}^2 + \frac{1}{\epsilon}(\dot{a}^2 + \Omega^2 a^2) + \epsilon U(X) + \epsilon a F(X) \tag{2.7}$$

and that as $|X| \to \infty$, $U \to 0$ and $F \to 0$ exponentially. The energy is thus asymptotically positive definite, and must be partitioned between X and a when the soliton is far from the defect.

This system corresponds to a particle X moving in an attractive potential well $\epsilon U(X)$ exponentially localized in a neighborhood of zero, coupled to a harmonic oscillator a by an exponentially localized term $\epsilon a F(X)$. Note that this model inherits many properties from the sine-Gordon system. $U(X)$ and $F(X)$ decay for large $|X|$, so that when $|X|$ is large $\ddot{X} \approx 0$ and the kink may propagate at any constant speed, independent of the impurity mode a, which oscillates at its characteristic frequency Ω. When X becomes small, the two equations become coupled and the kink may exchange energy with the impurity mode.

The variational method, while popular in the study of nonlinear optics, may contain significant pitfalls. First, it depends on the investigator finding an appropriate ansatz, as is done in Eq. (2.3). Second, even if the ansatz is chosen to be an exact representation of the initial data, there is no guarantee given by the method that the solution at a later time is well represented by an approximation of this form. Thus, one must carefully show that solutions of the full PDE system are well approximated by the ansatz.

Fig. 1 should be compared to Fig. 2. The former plots the output versus input velocities for the full PDE, as computed in [1]. It shows a critical velocity $v_c \approx 0.166$, and a finite number of resonance windows of decreasing

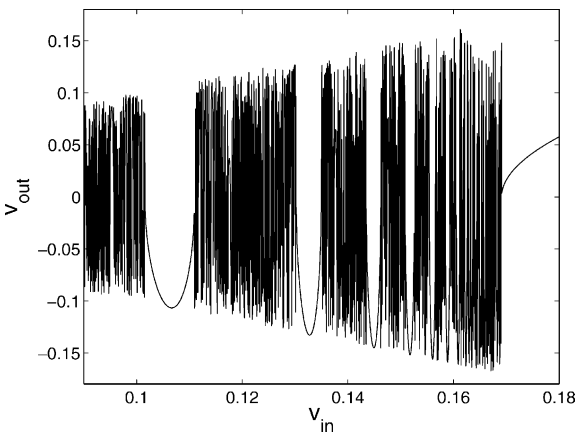

Fig. 2. The analog of Fig. 1 for the ODE (2.6), with $\epsilon = 0.5$.

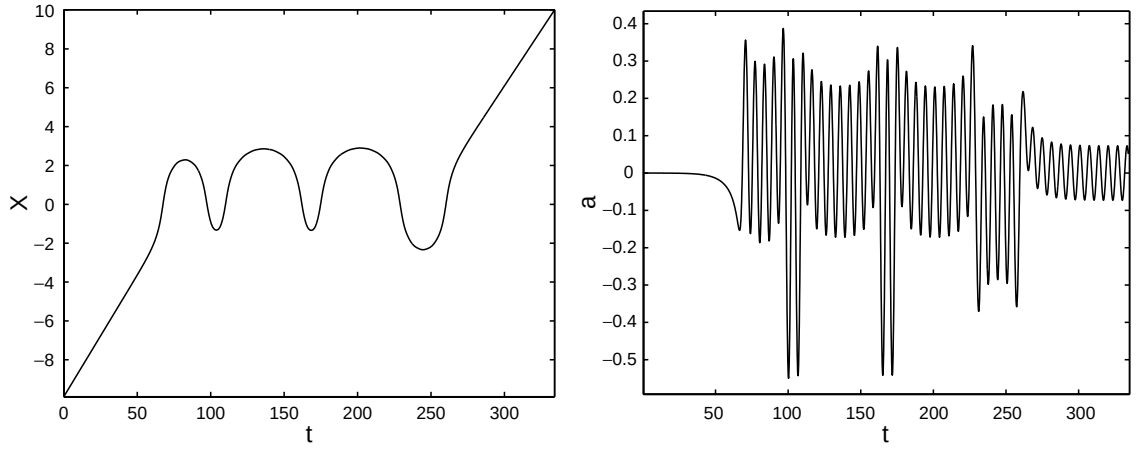

Fig. 3. $X(t)$ and $a(t)$ for the numerical experiment with $\epsilon = 0.5$ and $v_{\text{in}} = 0.125$.

width as $v \nearrow v_{\text{c}}$. In between these resonance windows, incoming solutions are trapped. For speeds slightly above v_{c}, it appears that $v_{\text{f}} = \text{O}((v_{\text{i}} - v_{\text{c}})^{1/2})$. The latter shows the same experiment for the ODE. This shows a critical velocity $v_{\text{c}} \approx 0.169$, in reasonable agreement with the PDE dynamics, a sequence of reflection windows, and a square-root profile just to the right of v_{c}. There are several major differences between the two numerical experiments. The PDE dynamics show only a finite number of resonance windows, while we will show the existence of an infinite number of resonance windows in the ODE dynamics. Solutions of the ODE with input velocities between the resonance windows are not, in general, captured for all time; as shown in [16], almost all solutions have nonzero v_{out}. The variational ODEs are Hamiltonian, and a variant of the Poincaré recurrence theorem implies that the set of initial conditions that are trapped has measure zero. The inter-window region contains infinitely many narrower windows, arising both from reflection and transmission. Finally, note that the exit speed in the resonance windows for the PDE computation is significantly smaller than the input speed, while for the ODE, the $v_{\text{out}} = -v_{\text{in}}$ at the center of the resonance windows. The variational ansatz (2.3) ignores energy that is lost via transfer to radiation modes. In [16], a dissipative correction to (2.6) is derived that takes this into account. This eliminates most of the sensitive dependence of v_{out} on v_{in} and replaces the chaotic regions with trapping regions. Nonetheless, we believe the Hamiltonian ODE (2.6) displays the fundamental features, if not the exact details, of the two-bounce resonance.

We now describe the structure of individual solutions to the ODE (2.6). The numerical experiments were performed with initial conditions

$$X(0) = -12, \qquad \dot{X}(0) = v_{\text{in}} > 0, \qquad a(0) = 0, \qquad \dot{a}(0) = 0.$$

For a general value of $v_{\text{in}} < v_{\text{c}}$, $X(t)$ comes in at constant speed, speeds up near zero, slows down as it approaches $+\infty$, oscillates back and forth a few times, then emerges and heads off in either direction with finite velocity v_{out}, with $|v_{\text{out}}| \leq v_{\text{in}}$. The harmonic oscillator $a(t)$, at first grows monotonically, and then begins oscillating, interrupted by a sequence of jumps in its amplitude and phase, before settling down to a steady oscillation as $X \to \infty$; see Fig. 3. This includes the v_{in} in the two-bounce resonance windows, in which the behavior is simpler: $X(t)$ approaches plus infinity, turns around, and heads back off to minus infinity and $a(t)$ grows, oscillates a finite number of time, and then shrinks again. At the very bottom of the resonance window (actually at a point tangent to the line $v_{\text{out}} = -v_{\text{in}}$ in Fig. 2), $a(t)$ actually returns all its energy to $X(t)$, so that $\lim_{t\to\infty} a(t) = 0$ and $v_{\text{out}} = -v_{\text{in}}$. In each successive window, the $a(t)$ undergoes one more oscillation than in the window to its left, with $n_{\min}(\epsilon)$ oscillations in the leftmost window. This number increases quickly as $\epsilon \searrow 0$. For example, when $\epsilon = 0.5$, $a(t)$

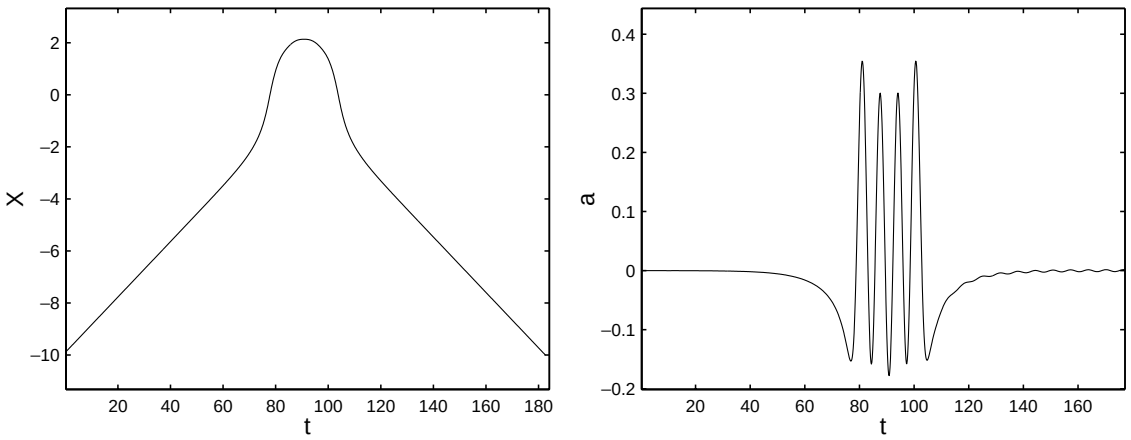

Fig. 4. $X(t)$ and $a(t)$ for the numerical experiment with $\epsilon = 0.5$ and $v_{\text{in}} = 0.10645$, showing the 2–4 resonance.

undergoes 4 oscillations for v_{in} in the leftmost window, 5 in the next window, etc.; see Figs. 4 and 5. The phrase "two-bounce resonance" was described above in Footnote 1; the equivalent of a "bounce" in this case occurs each time $X = 0$. We will refer to a 2 (*or* m) *bounce resonance* as a solution which crosses $X = 0$ 2 (m) times for which the output speed exactly equals the input speed and the amplitude of a approaches zero as $t \to \pm\infty$. We will refer to solutions with nearly resonant initial velocities, for which the soliton escapes after 2 (m) bounces, as 2 (m) *bounce solutions*. Thus in Fig. 4, the bounces occur when $X = 0$ at about $t = 80$ and $t = 100$. It is during the "bounces" that the kink is in contact with the defect and exchanges energy with the defect mode. During the first interaction, the soliton gives up energy to the defect mode and is temporarily trapped, and in the second, the energy is returned, and the soliton resumes propagating. We generalize this name to the 2-n bounce resonance, where n denotes the number of complete oscillations undergone by $a(t)$. It is possible to find in the simulations higher resonances, where soliton interacts with the defect three or more times, before its energy is returned and it resumes propagating. These resonance windows are naturally much narrower. Interspersed between the reflection and transmission windows is a set of initial conditions of measure zero in which the solutions are chaotic and $X(t)$ remains bounded for all time

It is helpful to look at projections of the solutions in the $(X, \dot{X})$ phase space. If we ignore the term $\epsilon a F'(X)$ in (2.6a), the simplified system has an elliptic fixed point at $(0, 0)$ and degenerate saddle-like fixed points at $(\pm\infty, 0)$,

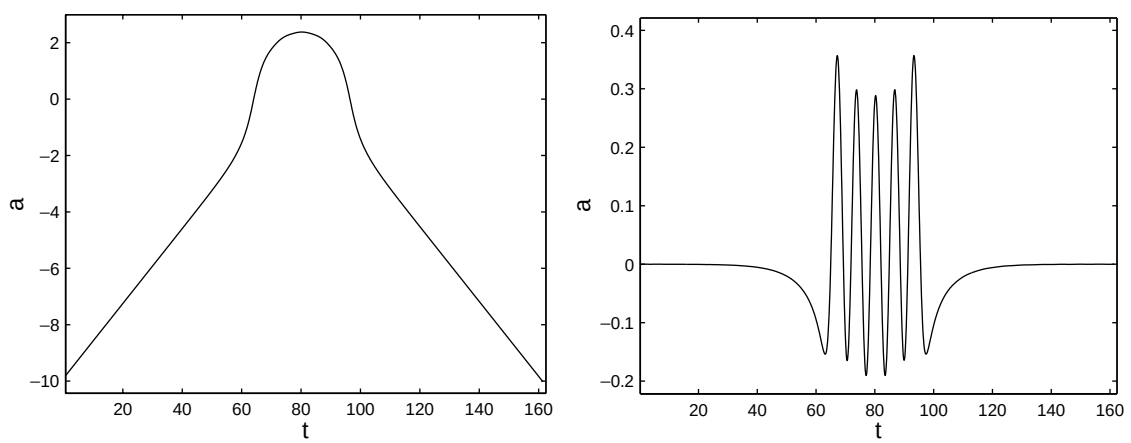

Fig. 5. $X(t)$ and $a(t)$ for the numerical experiment with $\epsilon = 0.5$ and $v_{\text{in}} = 0.1327$, showing the 2–5 resonance.

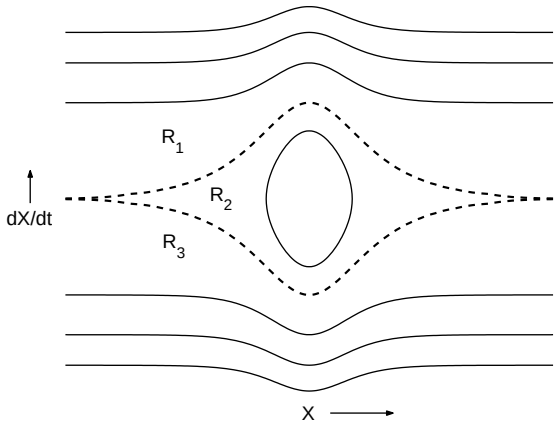

Fig. 6. The phase plane of the uncoupled X dynamics, divided into three regions by a pair of degenerate heteroclinic orbits.

connected by a pair of heteroclinic orbits, which split the phase space into three regions, as is shown in Fig. 6. In region R_1 (respectively R_3), solutions move right (respectively left) along trajectories that asymptote to horizontal lines for large $|X|$. Solutions in region R_2 oscillate clockwise, remaining bounded for all time. When the coupling to $a(t)$ is restored, these trajectories are no longer invariant, and the solution may cross over the separatrices. A typical solution starting in region R_1 will cross over the separatrix, oscillate inside R_2 several times, then exit to either region R_1 or R_3; as is shown in the first graph of Fig. 7. In a two-bounce solution, $X(t)$ must first cross from R_1 to R_2, undergo half an oscillation, and then cross into R_3 and propagate back toward $-\infty$; as is seen in the second graph of Fig. 7 for an illustration.

3. Determination of the critical velocity

To compute the critical velocity v_c, we will use a Melnikov computation [17,18]. Essentially, we write down the time rate of change of the energy contained in $X(t)$, and integrate this over a separatrix orbit to find the total energy transferred away from X as it travels from $-\infty$ to $+\infty$. If the initial energy is greater than the energy loss, then X reaches $+\infty$. If the energy is less, than the trajectory crosses the separatrix and turns around.

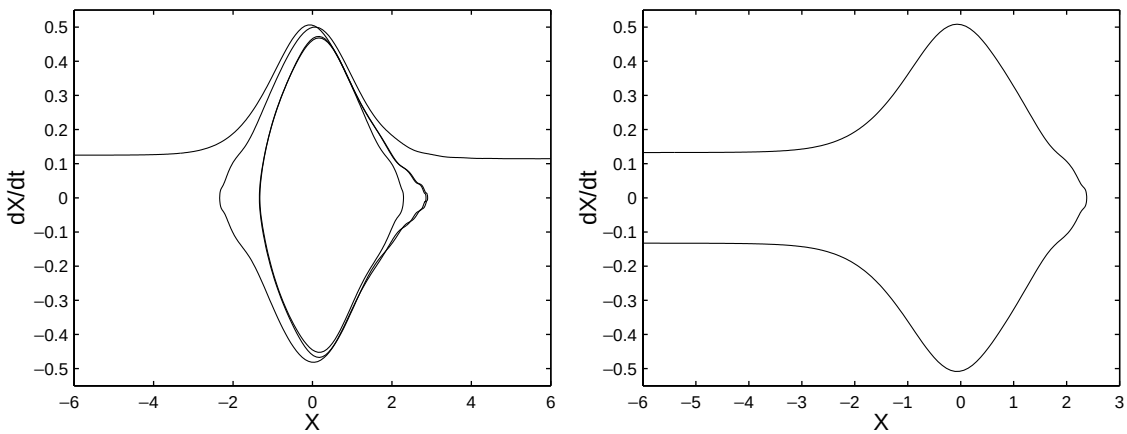

Fig. 7. Projections into $(X, \dot{X})$ plane of the solutions shown in Fig. 3 (left) and Fig. 5 (right).

We rescale the time variable $t \to \sqrt{\epsilon/2}t$. Under this scaling, the equations become:

$$4\ddot{X} + U'(X) + aF'(X) = 0, \tag{3.1a}$$

$$\ddot{a} + \lambda^2 a + \epsilon F(X) = 0, \tag{3.1b}$$

where

$$\lambda^2 = \frac{2}{\epsilon} - \frac{\epsilon}{2}. \tag{3.2}$$

This removes the explicit ϵ-dependence from (3.1a) and fixes the leading-order time scale.

We consider the initial value problem defined by (3.1) together with the "initial condition" that as $t \to -\infty$,

$$X \to -\infty, \qquad \dot{X} \to V, \quad a \to 0, \quad \dot{a} \to 0. \tag{3.3}$$

Because (3.1) is autonomous, this is insufficient to specify a unique solution, and we should append the condition that as $t \to -\infty$,

$$X \sim X_0 - Vt.$$

We use uppercase V to refer to velocity in the scaled system (3.1) and v to velocity in the original system (2.6). When $\epsilon = 0$, $a = \dot{a} = 0$ defines an invariant subspace $\mathcal{P}_0$ of (3.1) with trajectories confined to lie on surfaces along which the energy

$$E = 2\dot{X}^2 + U(X) \tag{3.4}$$

is constant.

As seen in Fig. 6, the unperturbed X-phase space features bounded periodic orbits for $E < 0$, unbounded orbits which tend to a finite velocity at $|t| \to \infty$ for $E > 0$ and separatrix orbits with $E = 0$ along which $\dot{X} \to 0$ as $|X| \to \infty$. Along this heteroclinic orbit

$$X = \pm \sinh^{-1}(t - t_1), \tag{3.5}$$

where t_1 is the "symmetry time" of the orbit at which $X(t) = 0$. In the calculation that follows, we will set $t_1 = 0$ for ease of notation. We will need to include nonzero t_1 later, and will reintroduce it at key locations in the computation.

When $\epsilon > 0$, $\mathcal{P}_0$ ceases to be invariant, and energy is transferred from X to a. Because the coupling term $F(X)$ decays exponentially, almost all the energy exchange takes place when X is small. This justifies calculating the change of energy along the separatrix, because very little of the change of energy takes place in the tails. We now compute the change in energy for small values of ϵ, as X travels from $-\infty$ to $+\infty$.

Using Eqs. (3.4) and (3.1a), the time derivative of the energy E is

$$\frac{\mathrm{d}E}{\mathrm{d}t} = (4\ddot{X} + U'(X))\dot{X} = -aF'(X)\dot{X}.$$

Integrating this over the separatrix orbit yields the approximate total loss of energy of the soliton over the trajectory in the form of a Melnikov integral:

$$\Delta E = \int_{-\infty}^{\infty} \frac{\mathrm{d}E}{\mathrm{d}t}\,\mathrm{d}t = -\int_{-\infty}^{\infty} F'(X(t))\dot{X}(t)a(t)\,\mathrm{d}t.$$

Plugging the various formulae into the separatrix (3.5) (using the plus signs for right-moving trajectories and allowing $t_1 = 0$, which does not effect this calculation):

$$F = -2\mathrm{sech}X \tanh X = -\frac{2t}{1+t^2}, \qquad F' = -4\mathrm{sech}^3 X + 2\mathrm{sech}X = -\frac{4}{(1+t^2)^{3/2}} + \frac{2}{(1+t^2)^{1/2}},$$
$$\dot{X} = \mathrm{sech}X = (1+t^2)^{-1/2}.$$

This gives the Melnikov integral

$$\Delta E = -\int_{-\infty}^{\infty} \left(\frac{-4}{(1+t^2)^2} + \frac{2}{1+t^2} \right) a(t)\,\mathrm{d}t. \tag{3.6}$$

We evaluate ΔE by first computing $a(t)$ and then using this in Eq. (3.6). Using initial condition (3.3), we may solve for a by variation of parameters:

$$a = \frac{\epsilon}{\lambda}\cos\lambda t \int_{-\infty}^{t} F(X(\tau))\sin\lambda\tau\,\mathrm{d}\tau - \frac{\epsilon}{\lambda}\sin\lambda t \int_{-\infty}^{t} F(X(\tau))\cos\lambda\tau\,\mathrm{d}\tau = -\frac{\epsilon}{\lambda}\int_{-\infty}^{t} F(X(\tau))\sin\lambda(t-\tau)\,\mathrm{d}\tau$$
$$= \frac{2\epsilon}{\lambda}\int_{-\infty}^{t} \sin\lambda(t-\tau)\frac{\tau}{1+\tau^2}\,\mathrm{d}\tau. \tag{3.7}$$

In fact, only the even component of $a(t)$ will be needed to evaluate ΔE. This is given by

$$a_{\mathrm{e}} = \frac{\epsilon}{\lambda}\int_{-\infty}^{\infty} \sin\lambda(t-\tau)\frac{\tau}{1+\tau^2}\,\mathrm{d}\tau. \tag{3.8}$$

This may be evaluated by introducing the complex exponential and closing the integral in the lower half τ-plane, which gives a contribution from the pole at $\tau = -\mathrm{i}$:

$$a_{\mathrm{e}} = -\frac{\epsilon\pi\,\mathrm{e}^{-\lambda}}{\lambda}\cos\lambda t. \tag{3.9}$$

This is small beyond all orders in ϵ, but the odd component of $a(t)$ contains algebraically small terms as well.

Then, putting (3.8) into (3.6) and using complex exponentials, gives

$$\Delta E = \frac{\pi\epsilon}{\lambda}\mathrm{e}^{-\lambda}\int_{-\infty}^{\infty}\left(-\frac{4}{(1+t^2)^2} + \frac{2}{1+t^2}\right)\mathrm{e}^{\mathrm{i}\lambda t}\,\mathrm{d}t.$$

This may be closed in the upper complex plane, where the residues at $t = \mathrm{i}$ leads to the final answer:

$$\Delta E = -2\pi^2\epsilon\,\mathrm{e}^{-2\lambda}, \tag{3.10}$$

where, recall, λ is defined by Eq. (3.2).

Note that a Melnikov integral has been evaluated to determine the leading order change of energy, essentially providing the first term in a formal series expansion of this change. In general the terms in such a series are algebraically small in the paramteter ϵ. Here the computed integral is $\mathrm{O}(\epsilon^{3/2}\,\mathrm{e}^{-\sqrt{2/\epsilon}})$, smaller than any power of ϵ. Formally, the next term in the series is will be proportional to some power of ϵ, arising, perhaps, due to algebraically small terms in the odd part of $a(t)$. Alarmingly, this or subsequent terms might dwarf the first term in the formal expansion, rendering the Melnikov integral meaningless. This concern was raised by Holmes et al. [19], who studied a related problem, the rapidly forced pendulum

$$\theta'' + \sin\theta = \epsilon^p \sin\frac{t}{\epsilon},$$

and were able to prove that for $p \geq 8$ the Melnikov integral accurately measures the exponentially small separatrix splitting. They were subsequently able to reduce the exponent p. Delshams and Seara [20] rigorously prove the

validity of the formal Melnikov analysis when the factor ϵ^p is replaced by an independent small parameter μ and give a more complete discussion of the history of this problem. We therefore have confidence that the Melnikov integral correctly measures the energy change. The numerical evidence of Section 6 is also shown to be in excellent agreement.

Eq. (3.10) may then be used to find the critical velocity[2]:

$$2\left(\frac{\mathrm{d}X}{\mathrm{d}t}\right)^2 = |\Delta E| = 2\pi^2\epsilon\,\mathrm{e}^{-2\lambda}, \tag{3.11}$$

$$V_\mathrm{c} \equiv \frac{\mathrm{d}X}{\mathrm{d}t} = \pi\sqrt{\epsilon}\,\mathrm{e}^{-\lambda}. \tag{3.12}$$

Recall that t has been scaled by a factor of $\sqrt{\epsilon/2}$. Removing this scaling gives a critical velocity

$$v_\mathrm{c} = \frac{\pi\epsilon}{\sqrt{2}}\mathrm{e}^{-\lambda}. \tag{3.13}$$

We may compute output velocity V_out for slightly supercritical input velocity $V_\mathrm{in} = \pi\sqrt{\epsilon}\,\mathrm{e}^{-\lambda}(1+\delta_V)$ using the energy:

$$2V_\mathrm{in}^2 - \Delta E = 2V_\mathrm{out}^2,$$

so that

$$V_\mathrm{out} \sim \sqrt{2\delta_V}V_\mathrm{c}.$$

This gives the characteristic square root behavior of the curve in Fig. 2 to the right of v_c.

We briefly mention two generalizations of the above Melnikov analysis that will be useful in later sections. On the first near-heteroclinic orbit, we assume that no energy resides in $a(t)$. On subsequent near-heteroclines, $a(t)$ is actively oscillating, so we first suppose that as $t \to -\infty$,

$$a(t) \sim \frac{2\epsilon\pi\,\mathrm{e}^{-\lambda}}{\lambda} A\cos\lambda(t-T), \tag{3.14}$$

where A and T will be determined later. Then, since Eq. (3.1b) is linear in $a(t)$, the contribution due to this term merely adds to the contribution already calculated. As before, only the even part of $a(t)$ is needed for the calculation. Thus using $\cos\lambda(t-T) = \cos\lambda T\cos\lambda t + \sin\lambda T\sin\lambda t$, the total change of energy is

$$\Delta E = (4A\cos\lambda T - 2)\pi^2\epsilon\,\mathrm{e}^{-2\lambda}. \tag{3.15}$$

Depending on the magnitude and sign of $A\cos\lambda T$ the energy change may be positive or negative.

Second, we consider the Melnikov integral computed along the separatrix in the lower half-plane. System (2.6) obeys the symmetry

$$(X, \dot{X}, a, \dot{a}; t) \to (-X, -\dot{X}, -a, -\dot{a}; t),$$

so that the Melnikov integral can be computed directly. Assuming the limiting behavior (3.14), the change of energy is

$$\Delta E = (-4A\cos\lambda T - 2)\pi^2\epsilon\,\mathrm{e}^{-2\lambda}. \tag{3.16}$$

[2] Recall that as $t \to -\infty$, $X \to -\infty$, so $U(X) \to 0$.

3.1. The full expansion of $a(t)$

In later sections, we will need more detailed knowledge of the form of $a(t)$. By Eqs. (3.7)–(3.9),

$$a = 2a_e - \frac{2\epsilon}{\lambda}\int_t^\infty \sin\lambda(t-\tau)\frac{\tau}{1+\tau^2}\,d\tau.$$

We obtain the asymptotic expression as $t \to +\infty$ by integrating by parts:

$$a(t) \sim \frac{2\epsilon}{\lambda^2}\left(\frac{t-t_1}{(t-t_1)^2+1} + O(\lambda^{-2})\right) - \frac{2\epsilon\pi\, e^{-\lambda}}{\lambda}\cos\lambda(t-t_1). \tag{3.17}$$

Similarly, as $t \to -\infty$,

$$a(t) \sim \frac{2\epsilon}{\lambda^2}\left(\frac{t-t_1}{(t-t_1)^2+1} + O(\lambda^{-2})\right), \tag{3.18}$$

with no exponentially small oscillatory term. Here we have re-introduced the dependence of the solution on the symmetry time t_1 from (3.5), ignored during the calculation above for transparency of notation. The algebraically small terms decay for large t, so as $t \to \infty$, it is the exponentially small oscillating term that dominates. However, when we use the method of matched asymptotic expansions, we will assume that t is exponentially large of the appropriate size so that the leading order algebraic term and the oscillation are of the same size.

4. Solutions near $|X| = \infty$

In the next two sections we construct matched asymptotic solutions to (3.1) by matching near-separatrix solutions to solutions valid near $|X| = \infty$. The solution for large $|X|$ may be expanded as a near-saddle approach to the degenerate saddle points at infinity. Nearly heteroclinic orbits alternate with near-saddle approaches. Near-saddle expansions for linear saddle points are common. In that case, exponential growth of solutions away from the saddle point matches to exponential decay of homoclinic orbits. Finite nonlinear saddle points corresponding to bifurcations for Hamiltonian systems have been analyzed by Haberman [8,9] and Diminnie and Haberman [10,11]. In the current work, the nonlinear saddle is at infinity, and we do not believe that such an expansion has been analyzed before. In the present case, solutions in the near-saddle region have finite-time singularities which match to the logarithmic growth of the heteroclinic orbits. We note from the conservative system (3.1) and expansion (3.17) that the contribution due to $aF'(X)$ is exponentially small for large t, so that to leading order

$$4\ddot{X} + U'(X) = 0, \tag{4.1}$$

with the energy given by (3.4). $U(X)$ may be approximated in a neighborhood of $\pm\infty$ by

$$U \sim -8\, e^{\mp 2X}.$$

We may then form approximations valid for large X in two different ways depending on whether the energy E is positive or negative. Phase portraits of (4.1), shown in Fig. 6, may clarify the results that follow.

If $E = 2V^2 > 0$, then the solution of (4.1) corresponding to the near-saddle approach is given by

$$e^{\pm X} = \pm\frac{2}{V}\sinh V(t-t_*) \quad \text{as } X \to \pm\infty. \tag{4.2}$$

The $\pm$ sign on the left side of the equation determines whether $X \to \pm\infty$, and the sign on the right must be chosen so that $\pm(t-t_*)$ is positive. The constant t_* is the finite blowup time at which time the right hand side approaches

zero, forcing $|X|$ to approach infinity. The V in the notation is used intentionally, as it gives the asymptotic velocity of the near-approach to the saddle.

The solution for the near-saddle approach with $E = -2M^2 < 0$ is given by

$$e^{\pm X} = \frac{2}{M}\cos M(t - t_{**}). \tag{4.3}$$

The solution $X(t)$ has finite-time singularities when $M(t - t_{**}) = \pm\pi/2$ and is even about the symmetry time $t = t_{**}$.

For large $|X|$, $F(X) \sim \mp 4\, e^{\pm X}$, so that from (3.1b),

$$\ddot{a} + \lambda^2 a \sim \pm 4\epsilon\, e^{\pm X}.$$

Since $\lambda \gg 1$, the asymptotic expansion of $a(t)$ is given by

$$a \sim \pm\frac{4\epsilon}{\lambda^2} e^{\pm X(t)} + c_1 \cos\lambda(t - t_1) + c_2 \sin\lambda(t - t_1), \tag{4.4}$$

where (4.2) or (4.3) may be used depending on the circumstance. Eq. (4.4) shows that near the saddle approaches $a(t)$ consists of simple harmonic oscillations about a slowly varying mean (which increases in forward and backwards time toward the finite time singularities), all of which can clearly be seen in the numerical calculations. The saddle approach with $E < 0$, described in detail in the next section must match backwards in time to (3.17), so that $c_2 = 0$ and $c_1 = -2\epsilon\pi\, e^{-\lambda}/\lambda$. Matching this near-saddle approach for $a(t)$ forward in time shows how this exponentially small oscillation is added as previously stated in (3.14).

5. Construction of solutions near the separatrix

We now construct an approximation to the initial value problem for the scaled model (3.1) under the assumption that the initial velocity is subcritical. To be precise, we consider the "initial value problem" defined by (3.1) and (3.3). We assume that $V > 0$ is less than the critical value found in (3.12). As the Melnikov function giving the energy change is exponentially small, we may make the assumption that $E(t)$ stays exponentially close to 0, its value along the heteroclinic orbit. $X(t)$ may be approximated in different way depending on $|X|$. These approximations may then be connected by their limiting behaviors to give a matched asymptotic expansion. When $|X| = O(1)$, it may be approximated by a heteroclinic orbit

$$X \approx \pm \sinh^{-1}(t - t_j),$$

where t_j is the "symmetry time" at which $X(t) = 0$ for the jth nearly heteroclinic orbit. For $|X|$ large, the solution is given by formulas (4.2) and (4.3). The exponentially small part of $a(t)$ contributes to the analysis, as it is needed to determine the energy difference between subsequent approaches to infinity.

5.1. The two-bounce solutions

The two-bounce solution can be constructed from the following pieces:

(1) A near-saddle approach to $X = -\infty$ with energy $E_0 = 2V_0^2$:

$$e^{-X} = -\frac{2}{V_0}\sinh V_0(t - t_*), \tag{5.1a}$$

with $V_0 < V_c$ as given by (3.12).

(2) A heteroclinic orbit with $\mathrm{d}X/\mathrm{d}t > 0$:

$$\sinh X = t - t_1. \tag{5.1b}$$

(3) A near saddle approach to $X = +\infty$ with negative energy $E = -2M_1^2$:

$$\mathrm{e}^X = \frac{2}{M_1}\cos M_1(t - t_{**}). \tag{5.1c}$$

(4) A heteroclinic orbit with $\mathrm{d}X/\mathrm{d}t < 0$:

$$\sinh X = -(t - t_2). \tag{5.1d}$$

(5) A near-saddle approach to $X = -\infty$ with positive energy $E = 2V_2^2$:

$$\mathrm{e}^{-X} = \frac{2}{V_2}\sinh V_2(t - t_{***}). \tag{5.1e}$$

The solution can be summarized as a succession of near-saddle approaches, connected by heteroclinic orbits. Since the change of energy between consecutive near-saddle approaches is given by (3.10), we see

$$-2M_1^2 - 2V_0^2 = -2\pi^2\epsilon\,\mathrm{e}^{-2\lambda}. \tag{5.2}$$

We now need to compute the change of energy along the second heteroclinic connection. We must first compute the symmetry time t_2 of the second heteroclinic orbit, which is done via leading order matching of $X(t)$. The algebraically small components of $a(t)$ can be obtained from $X(t)$ by regular perturbation, and thus match immediately once X satisfies matching conditions. The separatrix is given by $X = -\sinh^{-1}(t - t_j)$, and the oscillatory part of $a(t)$ is given by $-(2\epsilon\pi\,\mathrm{e}^{-\lambda}/\lambda)\cos\lambda(t - t_1)$ in backwards time. Shifting time by t_2, we arrive at the energy change computed in (3.16) with $A = -1$ and $T = t_2 - t_1$. The analytic criterion for a two-bounce solution is that the energy be positive after the second heteroclinic transition, i.e.

$$E_2 = 2V_0^2 - 2\pi^2\epsilon\,\mathrm{e}^{-2\lambda} + (4\cos\lambda(t_2 - t_1) - 2)\pi^2\epsilon\,\mathrm{e}^{-2\lambda} > 0. \tag{5.3}$$

If $E_2 < 0$, then the energy at this saddle approach is less than zero, and the solution does not escape at this saddle approach.

The large time singularity of the first heteroclinic orbit (5.1b):

$$\mathrm{e}^{-X} \sim \frac{1}{2}\frac{1}{t - t_1}$$

must match the singularity of (5.1c) as $M_1(t - t_{**}) \searrow -\pi/2$:

$$\mathrm{e}^{-X} \sim \frac{M_1}{2}\frac{1}{M_1(t - t_{**}) + \pi/2},$$

yielding

$$t_{**} - t_1 = \frac{\pi}{2M_1}.$$

A similar calculation yields

$$t_2 - t_{**} = \frac{\pi}{2M_1}.$$

Combining these gives

$$t_2 - t_1 = \frac{\pi}{M_1}. \tag{5.4}$$

Note that this is exactly half the period of a closed orbit with $E = -2M_1^2$. Matching (5.1a) and (5.1b) yields $t_* = t_1$, and matching (5.1d) and (5.1e) yields $t_{***} = t_2$.

5.2. The two-bounce resonance and the width of the two-bounce window

This does not suffice to determine resonant values of V_0, because we still need to satisfy the condition that the oscillatory component of $a(t)$ vanishes in component 5 of the solution. Thus, at this stage we require a matching condition on the exponentially small oscillating part of $a(t)$. Two-bounce resonant solutions are defined by the condition that $E_2 = 2V_0^2$. From (5.3), this requires that $\cos\lambda(t_2 - t_1) = 1$. Using (5.4), we obtain the analytic condition for two-bounce resonant solutions that

$$\frac{\lambda\pi}{M_1} = 2\pi n,$$

where $n > 0$ is an integer, so that $\Delta E = 2\pi^2\epsilon\,\mathrm{e}^{-2\lambda}$. Thus, the second jump in energy exactly cancels the first, and all of the energy is returned to the propagating mode X. This gives a quantization condition

$$M_1 = \frac{\lambda}{2n}. \tag{5.5}$$

We can combine this with Eq. (5.2), to obtain a formula for the initial velocity of the 2-n resonant solution

$$V_n = \sqrt{\pi^2\epsilon\,\mathrm{e}^{-2\lambda} - \frac{\lambda^2}{4n^2}}. \tag{5.6}$$

V_n denotes the (scaled) initial velocity of the soliton in 2-n resonance with the defect mode. In order that for V_n to be well-defined, n must satisfy

$$n \geq n_{\min}(\epsilon) \equiv \frac{\lambda\,\mathrm{e}^{\lambda}}{2\pi\sqrt{\epsilon}}. \tag{5.7}$$

This gives a lower bound on the number of a-oscillations in a two-bounce resonance and approaches infinity rapidly as $\epsilon \to 0^+$. This predicts that resonance windows disappear as ϵ is decreased, as is shown in the numerical study of Section 6 that follows.

We may find the width of the 2-n resonance window as follows. If the energy change along the second heteroclinic orbit satisfies $\Delta E > 2M_1^2$, then the solution has positive energy, the trajectory crosses the separatrix, and the soliton escapes. If $\Delta E < 2M_1^2$, then the solution remains bounded, and will approach minus infinity before turning around another time. Therefore, the boundaries of the 2-n window, as a function of M_1 are given by the values of M_1 where

$$\Delta E = 2M_1^2$$

in (5.3), i.e. if

$$\cos\frac{\lambda\pi}{M_1} = \frac{1}{2}\left(1 + \frac{M_1^2}{\pi^2\epsilon\,\mathrm{e}^{-2\lambda}}\right).$$

Letting $M_1 = \lambda/2(n+\delta)$, then

$$\cos 2\pi(n+\delta) = \cos 2\pi\delta = \frac{1}{2}\left(1 + \frac{n_{\min}^2(\epsilon)}{(n+\delta)^2}\right). \tag{5.8}$$

Considering first the width of the leftmost window, we let $n = \mathrm{int}(n_{\min}(\epsilon))+1$, then $\delta^2 = (1/2n\pi^2)(1-\mathrm{fr}(n_{\min}(\epsilon)))$, where $\mathrm{int}(Z)$ and $\mathrm{fr}(Z)$ are the integer and fractional parts of Z. Restricting our attention to the smaller windows closer to v_c, if $n \gg n_{\min}(\epsilon)$, then $\cos 2\pi\delta \approx 1/2$, or $\delta \approx \pm 1/6$. The left and right edges of the nth resonance window have velocity approximately

$$V_{n\pm} = \sqrt{\pi^2\epsilon\, \mathrm{e}^{-2\lambda} - \frac{\lambda^2}{4(n \pm 1/6)^2}}. \tag{5.9}$$

If n is sufficiently large, then $\delta_n = \lambda\, \mathrm{e}^{\lambda}/2\pi n\sqrt{\epsilon} \ll 1$, and we find that the width of the 2-n window is given by

$$W_n = V_{n+} - V_{n-} \approx V_c \delta_n^2 \left(\frac{3}{n}\right), \tag{5.10}$$

which scales as n^{-3} for large n.

5.3. The general initial value problem

If the second jump in energy, given by by the second Melnikov calculation (5.3), is less than $2M_1^2$, then the soliton does not escape on the second interaction with the defect. Instead it jumps to a new energy level inside the separatrix. We can then replace the sequence (5.1) with a finite number of nearly heteroclinic orbits separated by near saddle approaches (with negative energy) in which the solution usually escapes at the last saddle approach with positive energy:

(1) A near saddle approach to $X = -\infty$, with energy $E_0 = 2V_0^2$:

$$\mathrm{e}^{-X} = -\frac{2}{V_0}\sinh V_0(t - t_*). \tag{5.11a}$$

(2) A heteroclinic orbit with $\dot{X} > 0$, over which the change of energy is ΔE_1, given by the Melnikov integral (3.10):

$$\sinh X = t - t_1. \tag{5.11b}$$

(3) A near saddle approach alternating between $X = \pm\infty$, with energy $E_j = E_{j-1} + \Delta E_j = -2M_j^2$:

$$\mathrm{e}^{X} = \frac{2}{M_j}\cos M_j(t - t_*^j). \tag{5.11c}$$

(4) A heteroclinic orbit (alternating between $\dot{X} < 0$ and $\dot{X} > 0$):

$$\sinh X = \pm(t - t_j). \tag{5.11d}$$

After each nearly heteroclinic orbit, the energy is $E_{j+1} = E_j + \Delta E_j$. If $E_{j+1} < 0$, the solution solution has a near saddle approach with negative energy and hence returns to step 3. However, if $E_{j+1} > 0$, the solution escapes, and this last saddle approach is instead mathematically described by step 5.

(5) If the solution escapes (at velocity $\pm V_f$), then the near saddle approach at $x = \pm\infty$ satisfies:

$$e^{\pm X} = \frac{2}{V_f} \sinh V_f (t - t_{***}). \tag{5.11e}$$

Usually the solution will escape after a finite number of bounces. However, for a set of initial velocities of zero measure, the solution will consist of an infinite number of nearly heteroclinic orbits, will not escape, and will be chaotic. The interesting dynamics take place at step 3 above. We must again consider the oscillatory part of $a(t)$. In analogy with expansion (3.17), after j near-heteroclinic orbits, $a(t)$ may be written

$$a(t) \sim \text{algebraically small non-oscillatory terms} + \frac{2\epsilon\pi\, e^{-\lambda}}{\lambda} \sum_{k=1}^{j} (-1)^{k+1} \cos\lambda(t - t_k),$$

where we find $t_k - t_{k-1} = \pi/M_{k-1}$, the appropriate generalization of (5.4). The change in energy along the kth heteroclinic orbit is given by a generalization of Eqs. (3.15) and (3.16) to include multiple oscillating terms. If the solution contains exactly m heteroclinic connections, then the change of energy over all of the connections is given by the sum of the contributions over all the m nearly heteroclinic orbits, which, after some algebraic manipulation, is

$$\Delta E_{\text{total}} = 2\pi^2 \epsilon\, e^{-2\lambda} \sum_{i=1}^{m} \sum_{j=1}^{m} (-1)^{i+j+1} \cos\lambda(t_j - t_i). \tag{5.12}$$

The condition for a perfect m-bounce resonance in which $|v_{\text{in}}| = |v_{\text{out}}|$ is thus that $\Delta E = 0$, which will happen only for a measure zero set of initial velocities V_0. If this is the case, then $X(t)$ will have interacted with the defect a total of m times. Between each pair of bounces, $a(t)$ will have undergone an integer number of complete oscillations (plus a small phase shift). We may thus construct, in a manner similar to that above, the $m - (q_1, q_2, \ldots, q_{m-1})$ bounce window. Of course many of windows do not contain a complete resonance, i.e. there does not exist a velocity in the window for which all energy is returned to the propagating mode. When all the windows of initial conditions that eventually escape to $\pm\infty$ are removed, what remains is a Cantor-like set of initial conditions that are trapped for all positive time.

5.4. The three-bounce resonance

It is also possible to construct the three-bounce resonance solutions, which look like Fig. 8 in phase space. From (5.12), a three-bounce solution satisfies

$$\Delta E_{\text{total}} = 2\pi^2 \epsilon\, e^{-2\lambda} \left(-3 + 2\cos\frac{\lambda\pi}{M_1} + 2\cos\frac{\lambda\pi}{M_2} - 2\cos\left(\frac{\lambda\pi}{M_1} + \frac{\lambda\pi}{M_2}\right)\right).$$

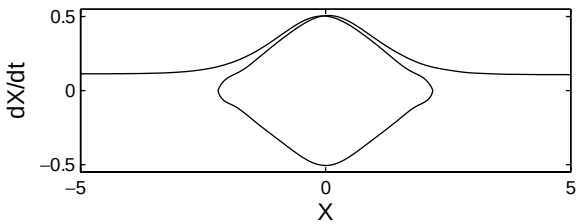

Fig. 8. A phase-plane portrait of a transmitted three-bounce solution of Eq. (3.1). Compare to reflected two-bounce solution of Fig. 7.

Three-bounce resonant solutions may be obtained by letting $\Delta E_{\text{total}} = 0$. Here we analyze this special case using symmetry. Note that the two-bounce solutions consist of X and a which are even functions of t (with the time origin shifted to be the midpoint between the two singularity times). Similarly (3.1) admits special solutions in which both $X(t)$ and $a(t)$ are odd. A three bounce resonant solution is an odd function of time, in which there are three energy jumps and $a(t) \to 0$ as $|t| \to \infty$. We may assume that the three singularity times are $-t_0$, 0, and t_0. Then we note that for the solution to be odd, the energy level E_1 for $t \in (-t_0, 0)$ must be the same as the energy level E_2 for $t \in (0, t_0)$, so $\Delta E = 0$ along the second heteroclinic orbit, i.e.

$$\Delta E = (4\cos\lambda t_0 - 2)\pi^2\epsilon\, \mathrm{e}^{-2\lambda} = 0.$$

Therefore $\cos\lambda t_0 = 1/2$ or

$$\lambda t_0 = 2n\pi \pm \tfrac{1}{3}\pi.$$

By our standard reasoning this gives

$$V = \sqrt{\pi^2\epsilon\, \mathrm{e}^{-2\lambda} - \frac{\lambda^2}{4(n \pm 1/6)^2}},$$

which is exactly the formula we obtained in (5.9) when we ignored a small term in that calculation. Therefore very close to the edge of each two-bounce window, on either side, there exists a symmetric three-bounce window. We may check that if before the second energy jump

$$a(t) \sim -2\cos(\lambda t \pm \tfrac{1}{3}\pi),$$

then afterward

$$a(t) \sim 2\cos(\lambda t \mp \tfrac{1}{3}\pi),$$

so the solution is odd, and we do not need to compute the third interaction. Although the three-bounce windows are too narrow to see with the naked eye, we were able to find them quite easily by looking carefully at the region around the above-determined velocities. In Fig. 9, we show $a(t)$ for the two three-bounce windows to the immediate

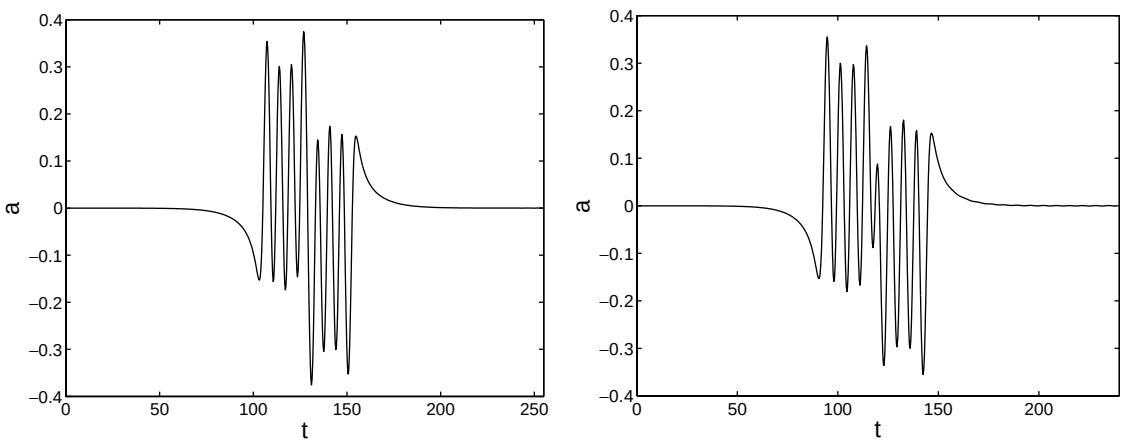

Fig. 9. The two three-bounce resonant solutions ($a(t)$ only) to the left and right of the first two-bounce window in Fig. 2: (a) $v = 0.09796$; (b) $v = 0.11301$.

left and right of the first two-bounce window shown in Fig. 2. Asymmetric three-bounce windows also exist, in which a oscillates a different number of times on the first approach to infinity than it does on the second. Although no transmission windows are seen in Fig. 1, they have been seen, albeit infrequently, in numerical simulations of the PDE [21].

6. Numerical verification

The analysis of the previous section has given us formulas by which we may compute several features of the solution, as a function of the defect strength ϵ. These include the critical velocity v_c (3.13), the minimum number of oscillations of $a(t)$ in a reflection window $n_{\min}(\epsilon)$ (5.7), and the locations and width of the two-bounce resonance windows ((5.6) and (5.10) after rescaling to the physical time and velocity scales).

6.1. Critical velocities

Fig. 10, shows the numerically computed critical velocities for the values $\epsilon \in \{1/8, 1/4, 1/2, 1\}$, as well as $v_c = \pi\epsilon \exp(-\lambda)/\sqrt{2}$. Of course, both the curve of calculated velocities, as well as the numerically computed velocities approach zero as $\epsilon \to 0$, so we must show they approach zero at the same rate to validate our theory. The lower half of the figure shows the ratio of the numerical and asymptotic values, which are correct to within 6% for $\epsilon = 1$ and to within 0.2% for $\epsilon = 1/8$.

6.2. Predicted minimum number of a-oscillations for resonance ($n_{\min}(\epsilon)$)

For the values $\epsilon = \{1/4, 1/2, 1\}$, formula (5.7) yields $n_{\min}(\epsilon)$ (rounded up to the nearest whole number): $n_{\min}(1/4) = 15$, $n_{\min}(1/2) = 4$, and $n_{\min}(1) = 1$, which are precisely the values found via numerical experiment. The formula gives $n_{\min}(1/8) = 98$. The fewest oscillations seen in the numerical experiments with $\epsilon = 1/8$ was 100, but the equations are very stiff when ϵ and v_{in} are very small, and smaller values of v_{in} were not investigated.

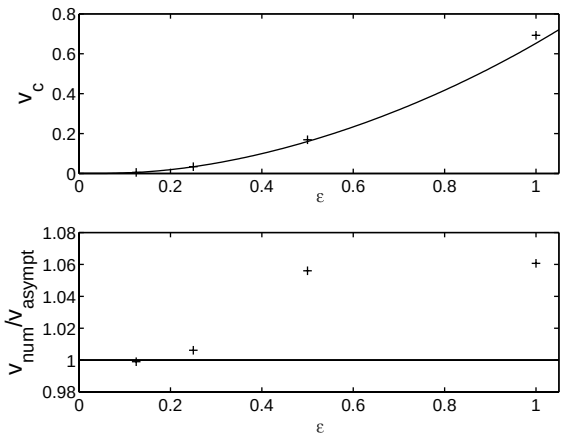

Fig. 10. (Top) Critical velocity as a function of ϵ, numerical $+$, and via asymptotic calculation (solid line). (Bottom) Ratio of numerical to asymptotic calculated values.

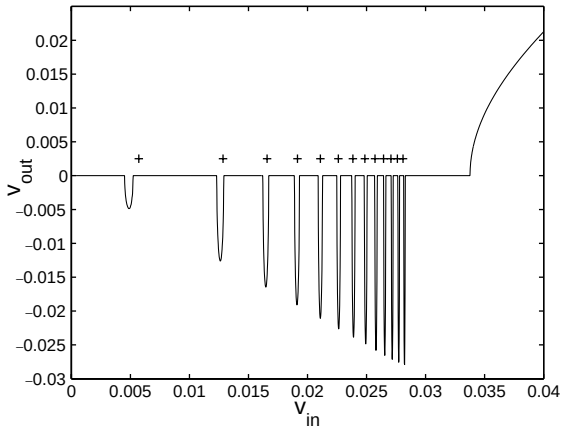

Fig. 11. Input vs. output velocities for $\epsilon = 1/4$ showing the predicted resonant initial velocities $+$. The chaotic scattering between the windows have been removed and only the first 13 windows are shown.

6.3. Resonance windows

The comparison of v_n with numerically computed values is shown in Fig. 11 for $\epsilon = 1/4$. Many of the resonance windows are well-predicted. We may gain more insight by considering Eq. (5.6) as defining n as a function of V (and hence as a function of the unscaled velocity v). In Fig. 12 we plot $\cos 2\pi n(v)$ as a function of v. If $n \in \mathbb{Z}$, then $\cos 2\pi n = 1$. Therefore the two-bounce resonance window centers (i.e. the resonant initial velocities) are given by the points where the curve $y = \cos 2\pi n(v)$ is tangent to the line $y = 1$. Eq. (5.8) (with $n + \delta$ replaced by $n(v)$) gives the edges of the resonance windows. Therefore to the immediate left and right of the resonance window centers, the curve $y = \cos 2\pi n(v)$ crosses the curve $y = (1/2)(1 + n_{\min}^2(\epsilon)/n(v)^2)$, giving the window edges. We note from the figure that this implies that the leftmost resonance windows should be narrowed with respect to the space between windows. This is confirmed in the plot of v_{out} vs. v_{in}.

Finally, the reasoning of Section 5.4 shows that the center of the three-bounce windows should be given by the intersection of the curve $y = \cos 2\pi n(v)$ with the line $y = 1/2$.

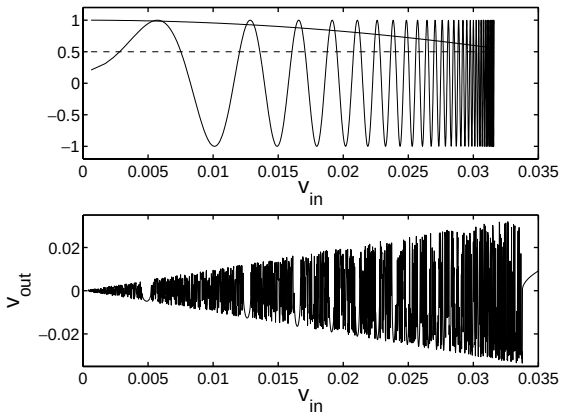

Fig. 12. (Top) The oscillatory curve is $y = \cos 2\pi n(v_{\text{in}})$ as a function of v_{in}. Its intersections with the line $y = 1$ (dotted line) give the location of the two-bounce resonant initial velocities. Intersections with the curve $y = (1/2)(1 + n_{\min}^2(\epsilon)/n(v)^2)$ (thick line) give the edges of the resonance windows. Intersections with $y = 1/2$ (dashed line) give the three-bounce resonant window velocities. (Bottom) The curve v_{out} vs. v_{in}.

7. Conclusions

We have shown how a resonant exchange of energy between a soliton and defect mode gives rise to two-bounce resonance windows. This was known to Campbell et al. as well as to Fei et al. However by applying perturbation techniques to a variational model of the system, we have been able to quantify this effect without recourse to statistical data fitting. The study of Fei et al. shows remarkable fits between the numerically determined locations of the resonance windows, and also gives an implicit equation for the critical velocity that is asymptotically equivalent to our Eq. (3.13). The chief advantage of our method is that we are able to determine the dependence of all these quantities on ϵ explicitly.

One of us has previously studied the model (2.6) in [16]. In that paper, ϵ was considered to be order 1 and an artificial parameter μ was introduced as a factor multiplying the coupling function $F(X)$. For small values of μ, we were able to show the dynamics contains a Smale horseshoe. In that construction, capture was identified with transfer of phase space between the regions of Fig. 6 via turnstile lobes in a certain Poincaré map. That Poincaré map was ill-defined as $\mu \to 1$, so the results were not directly applicable to Eq. (2.6), although were very suggestive of the dynamics. It does indicate how the dynamics in the regions between the resonance windows in Fig. 2 depends sensitively on the input velocity. Combining this with the quantitative information contained in the current study gives a rather complete picture of the dynamics.

Other studies of the two-bounce resonant phenomenon have often derived a formula for the resonance windows of the form

$$(v_c - v_n)^{-1/2} \sim nT + \theta_0,$$

where T is the period of the fast oscillations, and θ_0 is some offset time. The equivalent statement in this study is given in Eq. (5.5). This is equivalent to setting θ_0 to zero. To asymptotically compute θ_0 we would need to find further terms in (5.4), the equation for the time between interactions, in terms of the small energy-derived term M. The leading order term is $O(M^{-1})$ and symmetries of Eq. (4.1) show that the $O(1)$ term must be zero. The next term in the series is necessarily $O(M)$.

Many similar systems have shown the two-bounce resonance, and the methods developed here should be adaptable to such systems. However the current system is the simplest to study for several reasons. First, it depends explicitly on a small coupling parameter ϵ, and when $\epsilon \to 0$ decouples into two independent oscillators. Anninos et al. derive a variational model of the kink–antikink scattering in the ϕ^4 experiments of Campbell et al. [2,22]. This model does not depend explicitly on a small parameter, so an artificial one might need to be introduced. Since our formula for v_c is correct to within 6% even with $\epsilon = 1$, this may be a reasonable step to take. Other models do not decouple so cleanly as (3.1) as $\epsilon \to 0$. Nonetheless, in many systems it is possible to draw a diagram similar to Fig. 2, so we believe that a similar mechanism is at work.

Acknowledgements

We would like to thank Phil Holmes, Michael Weinstein, Greg Kriegsmann, and Chris Raymond for helpful discussions. RG was supported by NSF DMS-0204881 and by an SBR grant from NJIT.

References

[1] Z. Fei, Y.S. Kivshar, L. Vázquez, Resonant kink–impurity interactions in the sine-Gordon model, Phys. Rev. A 45 (1992) 6019–6030.
[2] D.K. Campbell, J.S. Schonfeld, C.A. Wingate, Resonance structure in kink–antikink interactions in ϕ^4 theory, Physica D 9 (1983) 1–32.

[3] M. Peyrard, D.K. Campbell, Kink–antikink interactions in a modified sine-Gordon model, Physica D 9 (1983) 33–51.
[4] D.K. Campbell, M. Peyrard, Solitary wave collisions revisited, Physica D 18 (1986) 47–53.
[5] D.K. Campbell, M. Peyrard, Kink–antikink interactions in the double sine-Gordon equation, Physica D 19 (1986) 165–205.
[6] R.H. Goodman, R.E. Slusher, M.I. Weinstein, Stopping light on a defect, J. Opt. Soc. Am. B 19 (2002) 1632–1635.
[7] Y. Tan, J. Yang, Complexity and regularity of vector–soliton collisions, Phys. Rev. E 64 (2001) 56616.
[8] R. Haberman, Slow passage through a transcritical bifurcation for Hamiltonian systems and the change in action due to a nonhyperbolic homoclinic orbit, Chaos 10 (2000) 641–648.
[9] R. Haberman, Slow passage through the nonhyperbolic homoclinic orbit associated with a subcritical pitchfork bifurcation for Hamiltonian systems and the change in action, SIAM J. Appl. Math. 62 (2001) 488–513.
[10] D.C. Diminnie, R. Haberman, Slow passage through a saddle-center bifurcation, J. Nonlinear Sci. 10 (2000) 197–221.
[11] D.C. Diminnie, R. Haberman, Slow passage through homoclinic orbits for the unfolding of a saddle-center bifurcation and the change in the adiabatic invariant, Physica D 162 (2002) 34–52.
[12] M.D. Kruskal, H. Segur, Asymptotics beyond all orders in a model of crystal growth, Stud. Appl. Math. 85 (1991) 129–181.
[13] A. Scott, Nonlinear science, in: Oxford Applied and Engineering Mathematics, vol. 1, Oxford University Press, Oxford, 1999 (emergence and dynamics of coherent structures, with contributions by Mads Peter Sørensen and Peter Leth Christiansen).
[14] D.W. McLaughlin, A.C. Scott, Perturbation analysis of flux on dynamics, Phys. Rev. A 18 (1978) 1652–1680.
[15] B.A. Malomed, Variational methods in nonlinear fiber optics and related fields, Progress Opt. 43 (2002) 71–193.
[16] R.H. Goodman, P.J. Holmes, M.I. Weinstein, Interaction of sine-Gordon kinks with defects: phase space transport in a two-mode model, Physica D 161 (2002) 21–44.
[17] J. Guckenheimer, P. Holmes, Nonlinear Oscillations, Dynamical Systems, and Bifurcations of Vector Fields, Springer-Verlag, New York, 1983.
[18] V.K. Melnikov, On the stability of the center for time periodic perturbations, Trans. Moscow Math. Soc. 12 (1963) 1–57.
[19] P. Holmes, J. Marsden, J. Scheurle, Exponentially small splittings of separatrices with applications to KAM theory and degenerate bifurcations, in: Hamiltonian Dynamical Systems (Boulder, CO, 1987), vol. 81 of Contemporary Mathematics, Am. Math. Soc., Providence, RI, 1988, pp. 213–244.
[20] A. Delshams, T.M. Seara, An asymptotic expression for the splitting of separatrices of the rapidly forced pendulum, Commun. Math. Phys. 150 (1992) 433–463.
[21] Y. Kivshar, Private communication.
[22] P. Anninos, S. Oliveira, R.A. Matzner, Fractal structure in the scalar $\lambda(\phi^2 - 1)^2$ model, Phys. Rev. D 44 (1991) 1147–1160.